Cement and Concrete Research 39 (2009) 1156–1163

Contents lists available at ScienceDirect

Cement and Concrete Research

journal homepage: http://ees.elsevier.com/CEMCON/default.asp

Effect of carbonation on the hydro-mechanical properties of Portland cements

A. Fabbri [a,*], J. Corvisier [a], A. Schubnel [a], F. Brunet [a], B. Goffé [a], G. Rimmele [b], V. Barlet-Gouédard [b]

[a] Laboratoire de Géologie, UMR 8538 ENS-CNRS, 24, rue Lhomond, 75005 Paris, France
[b] Schlumberger Riboud Product Center (SRPC), 1 Rue Becquerel, BP 202, F-92142 Clamart, France

ARTICLE INFO

Article history:
Received 23 December 2008
Accepted 30 July 2009

Keywords:
Characterization (B)
Microcraking (B)
Carbonation (C)
Elastic moduli (C)
Permeability (C)

ABSTRACT

We evaluate experimentally the effect of carbonation on the hydro-mechanical properties of Portland cement. Samples were carbonated at 90 °C and 28 MPa under wet supercritical CO_2. Two types of carbonation features were achieved, either the samples were homogeneously carbonated or they displayed sharp carbonation fronts. Using a tri-axial apparatus, the static elastic moduli and the mechanical strength were measured at in-situ pressure conditions (28 MPa) and showed a degradation of the mechanical properties of the samples where a carbonation front prevailed. Water and gas permeabilities were measured and showed that the samples with a carbonation front exhibit a stress sensitive permeability. P and S elastic wave velocities were measured to evaluate dynamic (ultrasonic range, 1 MHz) elastic moduli. The use of an effective medium theory approach enabled us to characterize the density and distribution of cracks within the samples. This approach outlines that the samples which developed a carbonation front were damaged.

1. Introduction

Underground CO_2 sequestration may be considered as an effective option only if the long-term integrity of the reservoirs can be insured. In this context, carbonation induced failure of the well-bore cement may create preferential carbon dioxide migration pathways back to the surface. The interaction between carbon dioxide and Portland cement at atmospheric pressure and temperature conditions is a relatively well-known phenomenon since it leads to the carbonation of the cement matrix and the corrosion of the reinforcements embedded in concrete (e.g., [1]). This interaction mainly consists in the chemical reaction of calcium hydroxide and calcium silicate hydrates with the carbon dioxide resulting in the initial matrix leaching, and the formation of calcium carbonates and water [2]. Since the carbonates that precipitate are less dense and exhibit higher mechanical properties than the cement matrix that is dissolved, atmospheric carbonation is known to decrease the overall porosity, change the permeability [3] and to increase the mechanical strength and the elastic moduli [4–6]. However, under downhole temperature and pressure conditions, the CO_2 is under its supercritical form, which changes the physico-chemical interactions that occur within the cement [7–12]. In particular, the interaction between cement and wet supercritical CO_2 (wet $scCO_2$) and/or CO_2 dissolved in water is drastically fasten up and is expected to change significantly the mechanical behaviour of the hardened cement paste [7,8,10,11,13]. Furthermore, laboratory experiments show that, when exposed to a CO_2-rich fluid at 90 °C and ca. 300 bars, Portland cements develop reaction fronts (carbonation and/or alteration) which involve the crystallisation of several $CaCO_3$ polymorphs [19].

In this paper, we propose a quantitative mechanical post-characterization of Portland cement samples exposed to wet $scCO_2$ at 90 °C and 28 MPa for several run durations. Using a tri-axial apparatus, static elastic moduli, P and S elastic wave velocity measurements (ultrasonic range, 1 MHz) and gas/water permeabilities were measured under confining pressure and deviatoric load, in dry and saturated conditions. The set of Portland cement samples were first reacted with wet $scCO_2$ beforehand in an autoclave under pressure (28 MPa) and temperature (90 °C), whereas subsequent tri-axial testing was carried out at room temperature on the recovered samples. An effective medium model developed by Fortin et al. [14] is used to interpret qualitatively the mechanical behaviour of the experimentally carbonated cement samples.

2. Experimental methods

2.1. Sample preparation

Cement slurry, with 0.44 water/cement ratio by mass (W/C), was vacuum-mixed according to API specification 10B, Section 5. Ordinary class G Portland cement according to the ISO 10426-1 International Standard and fresh water was used. Before mixing the slurry, an antifoam agent, a dispersant and a retarder were added to water in order

* Corresponding author. Present address: BRGM-GEO/G2R, 3, avenue Claude Guillemin, 45060 Orléans Cedex 2, France. Tel.: +33 2 38 64 32 79.
E-mail addresses: a.fabbri@brgm.fr (A. Fabbri), corvisier@geologie.ens.fr (J. Corvisier), aschubnel@geologie.ens.fr (A. Schubnel), brunet@geologie.ens.fr (F. Brunet), goffe@geologie.ens.fr (B. Goffé), grimmele@clamart.oilfield.slb.com (G. Rimmele), vbarlet@clamart.oilfield.slb.com (V. Barlet-Gouédard).

0008-8846/$ – see front matter © 2009 Elsevier Ltd. All rights reserved.
doi:10.1016/j.cemconres.2009.07.028

to optimize the main slurry properties. The cement was cast into 75 mm-diameter cylindrical moulds and cured for 72 h at 20.68 MPa and 90 °C in a curing chamber at SRPC (Clamart, France). Then, the specimens were cored and cut into cylindrical samples of 65-mm length and 30-mm diameter. Prior to the exposure to wet $scCO_2$, half of them were stored in fresh water (index w) while the other half was dried during a week in an oven at 85 °C +/− 5 °C (index d). Four sets of carbonated samples were obtained after a carbonation process that lasted 13, 35, 51, and 62 days at 28 MPa and 90 °C. The experimental set-up used here for cement carbonation under static conditions is described precisely in [10]. The conditions of 28 MPa and 90 °C have been chosen for their relevance to deep geological storage. Hardened cement samples (two dried and two wet samples) were positioned in the upper part of the autoclave in a wet supercritical CO_2 environment. They are supported by samples immerged in water which are not studied here (cf. Fig. 1). At the end of the carbonation stage, the depressurisation phase starts from 28 MPa down to 5 MPa in 6 h and from 5 MPa down to atmospheric pressure in 1 h.

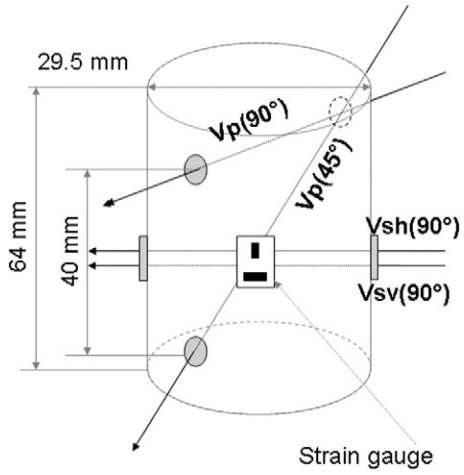

Fig. 2. Schematic representation of the specimen set-up. Strain gauges are represented in black and the piezoelectric transducers in light grey. Vp stands for compressional waves while Vsh and Vsv stand for respectively the horizontal and vertical shear waves.

2.2. Experimental set-up

After the carbonation process and prior to the tri-axial testing, core sample surfaces were rectified and polished to ensure perfect parallelism and minimum friction. The samples were dried in an oven at 85 °C +/− 5 °C until they reached a constant mass. They were then kept dried in a hermetic bell jar. Longitudinal and orthoradial strains (noted ε_{zz} and $\varepsilon_{\theta\theta}$ respectively) were measured using strain gauges (TML FLA-20, Tokyosokki) glued directly onto the sample surface. Seven piezoelectric transducers (PI ceramic PI255, 1 MHz resonance) were also glued on the cylindrical sample in order to measure two different P, and two different S ultrasonic wave velocities. The schematic representation of the specimen set-up is reported in Fig. 2. In the following, we did not investigate elastic wave anisotropy and only average P and S velocities will be discussed. Velocities were calculated measuring the time of flight needed for an acoustic pulse to travel across the sample. For each measurement, hundred waveforms were stacked on a digital oscilloscope, in order to increase the signal/noise ratio. The software InSite (ASC Ltd.) was used to monitor and process the digital waveforms. In particular, the arrival time was estimated using a cross-correlation technique. In such conditions, the absolute arrival time error was of the order of a few percent, but the relative error between the master velocity survey and the following ones was lowered to ~0.1%. Waveforms of the dried non-carbonated sample under a confining pressure of 30 MPa were chosen as our master survey reference for cross-correlation.

Water and argon gas permeabilities were measured using the constant flow technique provided by a high precision double microvolumetric pump (Quizix Qx20k). Applying a constant pressure difference ($\Delta P = 1$ MPa) at the top and bottom of the sample, the flow through the specimen was calculated from the volume variation of the pumps ($Q = dVpump/dt$). When the upstream and downstream flow became equal (about half an hour for gas and 2 h for water), the

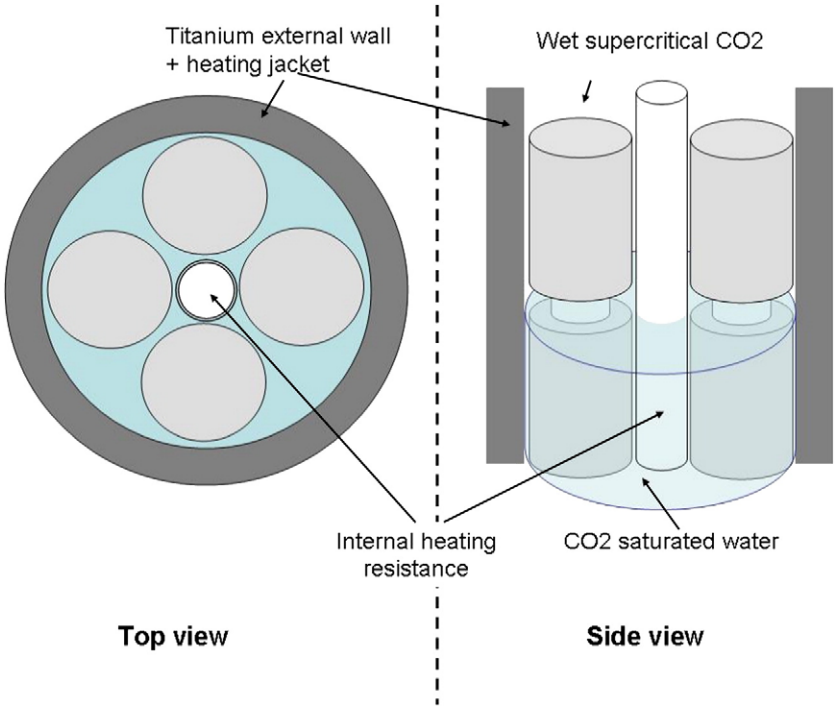

Fig. 1. Schematic representation of the experimental set-up used for cement carbonation.

steady state was supposed to be reached and permeability was estimated using Darcy's law:

$$\kappa = \frac{Q\eta l}{S\Delta p} \quad (1)$$

where η is the viscosity of the fluid (at 20 °C and 28 MPa, $\eta = 1.02$ mPa s for water and $\eta = 30.8$ μPa s for argon gas; [15]), l is the specimen length, and S is its cross-sectional area. Switching the flow direction in the sample, two symmetrical measurements were systematically performed.

The tri-axial cell at the Laboratoire de Geologie (ENS) was previously precisely described in [16,17]. The standard test procedure started with a confining pressure ($\sigma_c = \sigma_{ii}/3$) load, from 0 to 30 MPa. During this confinement stage, the evolution of the dynamic bulk (K) and shear (G) moduli were monitored using the evolution the P and the S elastic wave velocities (V_p and V_s respectively):

$$G = \rho_d V_s^2 \text{ and } K = \rho_d\left(V_p^2 - \frac{4}{3}V_s^2\right). \quad (2)$$

At a confining pressure of 30 MPa, an axial deviatoric stress loading ($\sigma_d = \sigma_{zz} - \sigma_c$), from 0 to 30 MPa, was applied. This led to the estimation of the dry Young's modulus E_d and Poisson's ratio ν_d through:

$$E_d = \frac{9KG}{3K+G} = -\left.\frac{\partial\sigma_d}{\partial\varepsilon_{zz}}\right|_{\sigma_c} \text{ and } \nu_d = \frac{3K-2G}{6K+2G} = -\left.\frac{\partial\varepsilon_{\theta\theta}}{\partial\varepsilon_{zz}}\right|_{\sigma_c}. \quad (3)$$

These two moduli were also estimated in the dynamic range, from ultrasonic velocities (index u in Table 2).

In a second stage, the deviatoric stress was unloaded and the argon pore pressure was progressively increased and stabilized to 28 MPa for at least 2 h, in order to reach a full saturation allowing gas permeability measurements. The next step consisted in the sample water saturation at a pore pressure of 28 MPa which required at least 12 h. Applying an increasing axial deviatoric stress, the specimen was eventually loaded to failure. Drained elastic constant E_w and ν_w were estimated and the water permeability was measured at 0 MPa, 30 MPa and 50 MPa axial deviatoric stresses. At the end of each experiment, the sample was carefully unloaded in order to analyze the fracture geometry.

3. Experimental results and discussion

3.1. Results of sample carbonation

As expected, the wet samples led to annular carbonation (AC) with a sharp carbonation front [10]. Typical for a diffusion front, the thickness of the carbonated rim increases linearly with the square root of time [9,10]. However, as shown in Fig. 3, the previously dried specimens show homogeneous carbonation (HC) through the whole sample, i.e. with no visible front. Since carbonation fronts arise from a process which is mainly limited by the diffusion of aqueous species (CO_2 inward and Ca^{2+} outward) [18], homogeneous carbonation can be understood by the rapid diffusion of wet $scCO_2$ throughout the unsaturated porous network of the dried specimens.

Mineral characterization and porosity distribution in AC cement samples exposed to CO_2 fluids under pressure and temperature have already been the subject of intensive studies [7,10,19] and only HC samples will be further characterized here using Raman microspectrometry (Renishaw InVia using a 785 nm IR diode laser at ENS) and scanning electron microprobe (Hitachi S-2500 equipped with EDS at ENS) on polished sections as well as X-ray powder diffraction (XRPD, Rigaku, rotating Cu-anode at ENS). The carbonation features in HC samples are roughly similar to those described in the carbonated zone for AC cement: portlandite is carbonated and calcium silicate hydrates (CSH) have transformed into Ca-carbonates and a silica-rich phase (Fig. 3). Nevertheless, XRPD data indicate partial carbonation since very low amount of portlandite, occurring as relict, is detected after 35 and 65 days of experimental carbonation (Fig. 4). Furthermore, the microtexture of HC samples is different to that of AC (Fig. 4). Both XRPD and Raman microspectrometry clearly show that contrary to AC samples, $CaCO_3$-vaterite is not preserved (or has not nucleated) in HC samples and only calcite and aragonite are observed (Fig. 5). Aragonite and vaterite are metastable $CaCO_3$ polymorphs under the considered downhole conditions [20] where only calcite is expected. However, as showed by [19], their occurrence in the experimentally carbonated sample is an evidence for a strong chemical disequilibrium between the cement sample and the CO_2-rich fluid which favours the crystallisation of metastable polymorphs with nucleation kinetics higher than that of the stable form (i.e. calcite).

Density, water porosity and carbonation-front thickness (when present) of our samples are summarized in Table 1 where t_c is the carbonation time, ϕ is the water porosity (evaluated from the sample mass difference between dried, at 85 +/− 5 °C, and saturated states), ρ_d is the density of the dried specimen and e_c is the thickness of the carbonation front. Table 1 highlights that the carbonation process leads to a reduction of porosity and an increase of dried density, which thus shows that both mass and volume of the carbonates which precipitate are higher than the one of the dissolved and/or leached cement solid matrix.

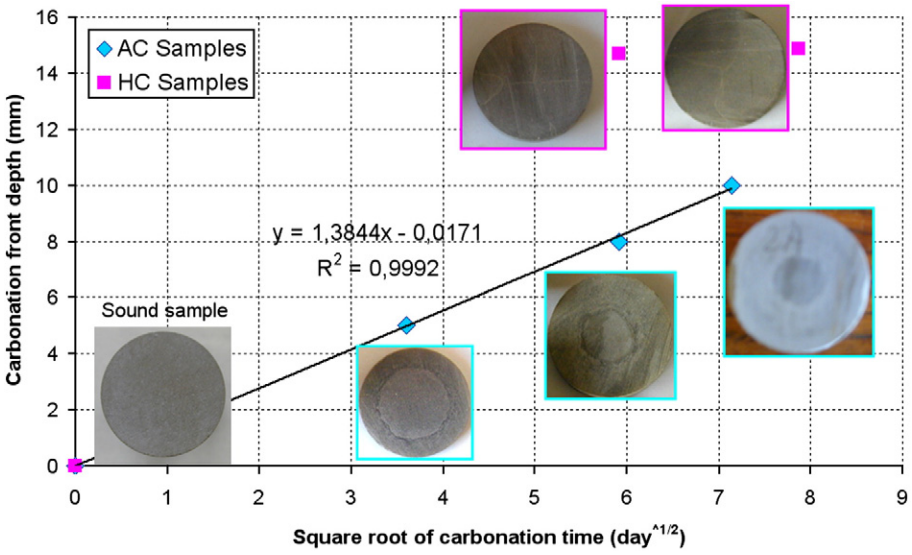

Fig. 3. Evolution of the AC and HC sample carbonation front versus the square root of carbonation time.

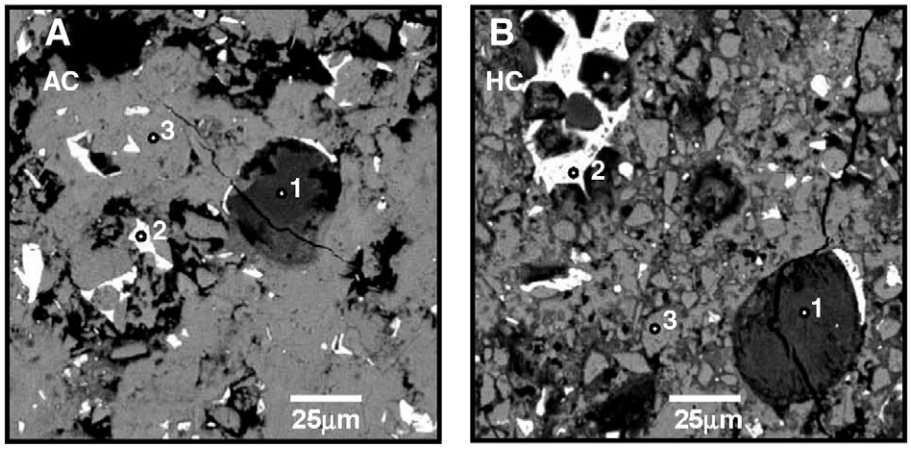

Fig. 4. Scanning electron microscope images (back-scattered electron) of (A) the carbonated zone of the sample P51w (1: SiO_2, 2: C_4AF and 3: $CSH + CaCO_3$) and (B) sample P35d (1: SiO_2, 2: C_4AF and 3: $CSH + CaCO_3$).

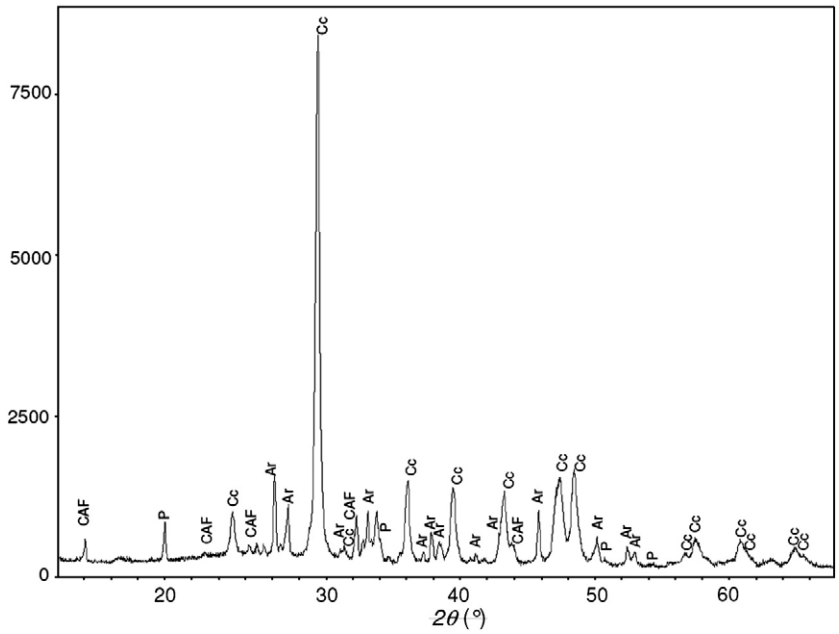

Fig. 5. XRPD data for the HC sample P35d (CuKα) (CAF: C4AF, P: portlandite, Cc: calcite and Ar: aragonite).

3.2. Mechanical characterization tests results

The evolutions of elastic wave velocities and the resulting *K* and *G* moduli during the confinement stage in dry conditions are reported in Fig. 6A, B and C respectively. No significant variations were observed on non-carbonated (PO) and HC samples (P35d, P62d). In contrast, the elastic wave velocities and the *K* and *G* moduli of AC (P13w, P51w and P62w) samples revealed significant pressure sensitivity up to a critical pressure (p_c) of approximately 15 MPa. In rock physics, such a pressure sensitivity of the dynamic elastic moduli is commonly interpreted as due to the elastic closure of micro-cracks. Indeed, at a given confining pressure (p_c), all crack of aspect ratios lower than $\zeta = w/c \propto pc/E$ [21] are expected to be closed. Here, *E* is the cement matrix Young's modulus, *w* is the crack average half-aperture, and *c* is the crack distribution average radius. In that case, at a confinement pressure of 15 MPa, all cracks of aspect ratio lower than 10^{-3} should be closed under the effect of the confining pressure.

Table 1
Sample characterization.

	AC/HC	t_c days	ϕ %	ρ_d g/cm^3	e_c mm
P0	–	0	41	1.53	–
P13w	AC	13	33	1.80	5
P35w	AC	35	29	1.90	8
P51w	AC	51	28	1.95	10
P62w	AC	62	31	1.87	11
P35d	HC	35	26	1.99	–
P62d	HC	62	24	2.03	–

Commonly, elastic wave velocity and dynamic elastic moduli evolution can be interpreted in terms of porosity and crack density (d_f) using an effective medium theory approach. Numerous models exist in the literature (e.g. [22,23]), but one of the simplest cases is that of the non-interactive approach, where stress and strain interactions between inclusions are neglected. Although such an approximation is valid for low porosities and crack densities only, it might be particularly well suited for the case of damaged cements, where such a dual porosity is likely to prevail. This technique has the advantage to separate the effects on the elastic properties of the compliant porosity (i.e. cracks which close under the effect of pressure) and the non-compliant (equate pores that are pressure insensitive). Using such a framework and assuming penny-shaped

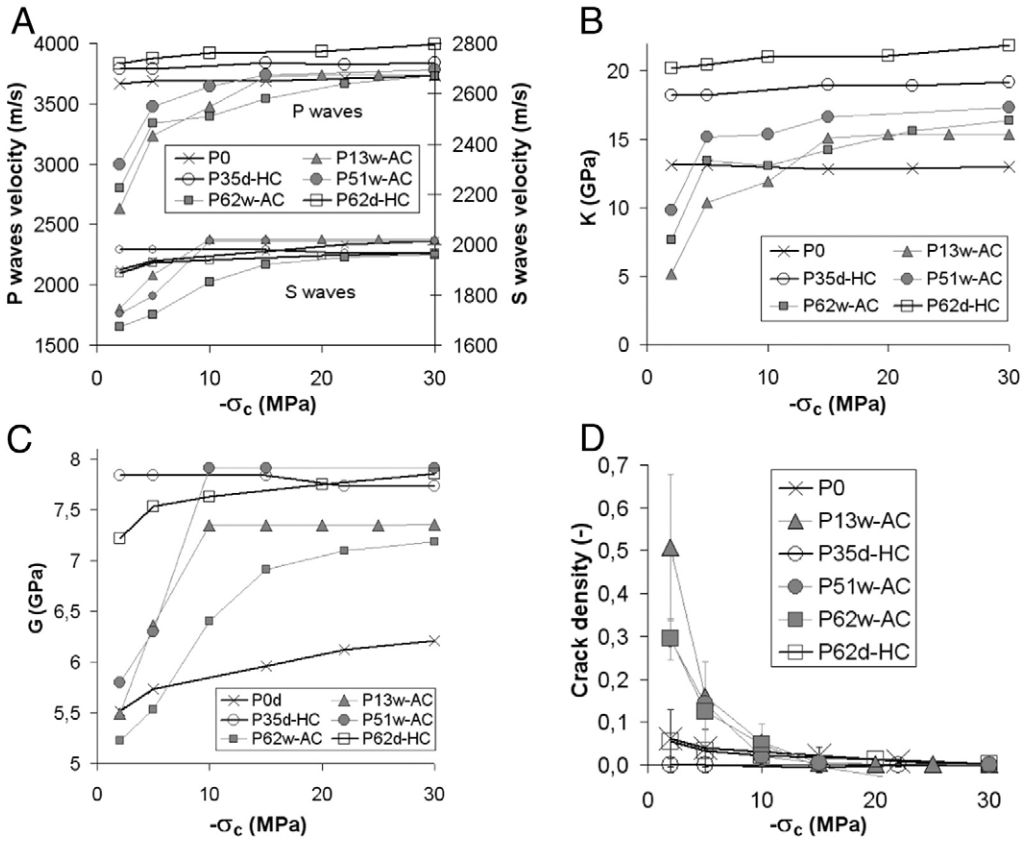

Fig. 6. Evolution of (A) P and S wave velocities, (B) bulk modulus, (C) shear modulus and (D) crack density versus the confining pressure σ (c). PO corresponds to the non-carbonated samples, black thick lines to HC samples and grey thin lines to AC samples.

geometry for the cracks, Fortin et al., [14] showed that the bulk and shear effective moduli of a material could be rigorously expressed in terms of the material's matrix elastic properties, a scalar accounting for crack density and the porosity only:

$$\frac{K_m}{K} = 1 + \frac{d_f}{1-\phi}\frac{h(2-\nu_m)}{2(1-2\nu_m)} + \frac{\phi}{1-\phi}\frac{3(1-\nu_m)}{2(1-2\nu_m)} \quad (4a)$$

$$\frac{G_m}{G} = 1 + \frac{d_f}{1-\phi}\frac{h(5-\nu_m)}{5(1-2\nu_m)} + \frac{\phi}{1-\phi}\frac{15(1-\nu_m)}{7-5\nu_m} \quad (4b)$$

where $K_m = K_{30}(1+(3/2)\ \phi/(1-\phi)\ (1-\nu_m)/(1-\nu_m))$, $G_m = G_{30}(1+15\phi/(1-\phi)\ (1-\nu_m)/(7-5\nu_m))$, $\nu_m = (3K_m - 2G_m)/(6K_m + 2G_m)$ and $h = 16(1-\nu_m^2)/9/(1-0.5\nu_m)$. The crack density is a scalar defined by $\rho = \frac{1}{V}\sum_0^N c_i^3$, where c_i is the radius of the ith crack, N being the total number of cracks embedded in the representative elementary volume V. For a distribution of penny-shaped cracks with constant aspect ratio, the total micro-crack porosity can be expressed as $\phi_{mc} = \pi\rho w/c$. K_{30} and G_{30} are respectively the bulk and the shear modulus of the intact specimen. For sake of simplicity, we assume these to be equal to the moduli measured at 30 MPa confining pressure. The crack density variation is then reported in Fig. 6D. The d_f values of AC samples at $-\sigma_c = 2$ MPa, ranges from 0.3 to 0.5. The permeability percolation threshold being reached at crack densities of 0.14 only, this last observation leads us to the conclusion that, at this low confinement, micro-cracks network are likely to become an important pathway for CO_2 migration. This is not the case for non-carbonated and HC samples where d_f always remains lower than 0.1.

The results of hydro-mechanical characterization are reported in Fig. 7A and C for HC samples, in Fig. 7B and D for AC samples and summarized in Table 2. Whatever the characterization test (dry tri-axial, drained tri-axial or dry ultrasonic), the Young's modulus of HC samples (P35d and P62d) are significantly higher than those of the non-carbonated samples. This result is in agreement with former studies which have shown an increase of cement Young's modulus due to carbonation [6]. However, the Young's modulus of AC samples remains close to those of uncarbonated samples (except for P13w). For the drained saturated case, the Young modulus of all AC samples is even lower than that of uncarbonated samples. In light of the microtextural data on AC cements [7,10], this feature may be explained by the presence of a dissolution zone (high porosity) just beyond the carbonation front. It is expected that cracks should easily nucleate at the corresponding interface, because of elastic strain incompatibilities between two media of different compliance. The increase of pore pressure could then re-open these cracks which were closed during the confining stage. In this case, the difference in Young's modulus between AC and HC samples is commonly more pronounced under drained saturated conditions than under dry conditions.

Water (κ_w) and gas (κ_{ar}) permeability measurements are reported in Table 2. For the AC samples, the permeability decreases as the carbonation-front thickness increases and the variation between P13w, P35w and P62w samples seems to be linear with the ratio of the carbonated cross-surface. However, in contrast to non-carbonated and HC samples, the application of a deviatoric load was found to increase significantly the permeability (Fig. 8A). A difference is observed between the gas and water permeabilities (κ_w/κ_{ar} is about 7 for the sound sample and about 2.5 for carbonated samples). It is commonly attributed to the differences between water/solid and gas/solid interactions, slip effects during gas permeability measurement, etc… [24]. As the leaching of the cement matrix and the carbonate precipitation act on these physico-chemical processes, it is not surprising that the difference between κ_w and κ_{ar} is not the same for all the samples. As a consequence, the permeability of carbonated cements under downhole conditions is likely to be stress sensitive and

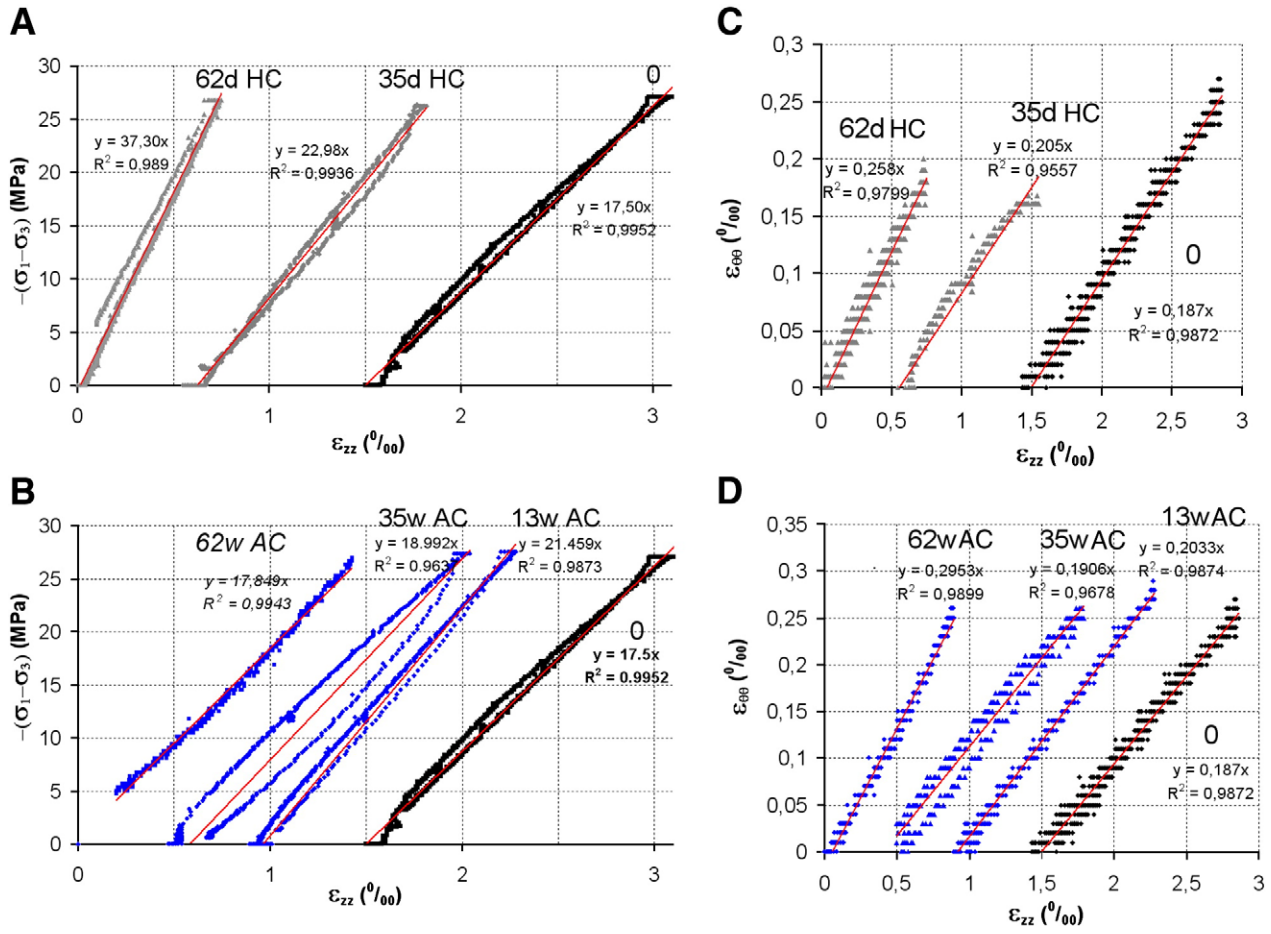

Fig. 7. σ_d–ε_{zz} (A, B) and $\varepsilon_{\theta\theta}$–$\varepsilon_{zz}$ (C, D) experimental curves during the deviatoric load of dry samples. To increase the graph readability the curves are artificially shifted.

in cases where a deviatoric stress is present, the permeability of the cement can be higher than expected. This result is consistent with the failure shape of the tested samples (cf. Fig. 8B). Indeed, while the non-carbonated sample exhibits 45° oriented cross fractures commonly observed during tri-axial loading experiments, the AC samples reveal vertical fractures surrounding the carbonation front. Finally, summarized on Table 2, the strength (f_{rupt}) of AC samples is lower than that of the uncarbonated cement. This is not the case for the HC samples for which no clear tendency is observed: the P35d paste revealed strength of 80 MPa while P62d failed at 57 MPa deviatoric stress.

3.3. Discussion

All these results indicate that AC samples were damaged during or after the carbonation process at 28 MPa. Crack formation in the course of depressurisation of the autoclave after carbonation at 28 MPa cannot be ruled out. One can then wonder why AC samples were much more damaged than HC samples, although they were submitted to the same depressurisation procedure. This significant increase of the porous space localised at the carbonation front has been also observed by Rimmele et al., [7] and Corvisier et al. [19]. This may be due to the stiffness contrast between the carbonated and the dissolution zones in AC samples, at the interface of which cracks (and failure) are expected to occur. Another possibility being that fracturing could occur as a response to the carbonation process itself. Schematically, this process can be divided into two major steps: (1) the dissolution of the cement matrix by the acidic CO_2-rich fluid and (2) carbonate precipitation. Reaction (1) engenders water production and an increase of porosity whereas overall reaction (2) produces a global reduction of porosity, because the carbonate volume is higher than the volume of the cement phases which are consumed. If the precipitation process is fast enough and localised, a significant pore overpressure could happen concurrently and induce damage of the solid matrix. It is here emphasized that damage will increase with decreasing density of the carbonate precipitate. It is then consistent with the fact that vaterite (with a density of 2.5 g/cm^3) is observed on the damaged carbonated front of AC samples while only calcite and aragonite (with a density of 2.7 g/cm^3 and 2.9 g/cm^3, respectively) are observed on less-damaged HC samples. To illustrate this point, let us consider the pore scale model described in [26], which is composed of a pore of radius $R = 500$ nm, connected from other pores through a capillary of radius $r = 1$ nm and length $L = 250$ µm. Let us note $S_p = 6\ 10^6$ m^2/m^3 the specific surface area of the pore, $V_{vaterite} = 40$ cm^3/mol the molar volume of the vaterite that

Table 2
Hydro-mechanical properties of the hardened cement pastes.

	AC/HC	E_d GPa	ν_d –	E_u GPa	ν_u –	E_w GPa	ν_w –	κ_{ar} u	κ_w u	f_{rupt} MPa
P0	–	17.5	0.19	16.1	0.29	16.4	0.24	7.1	1.0	63
P13w	AC	21.5	0.20	19.0	0.29	17.4	–	5.2	2.4	50
P35w	AC	19.0	0.20	18.5	0.31	13.4	0.18	3.3	1.3	57
P51w	AC	19.1	0.22	20.6	0.30	–	–	–	–	–
P62w	AC	17.8	0.30	18.8	0.31	15.4	0.33	1.7	0.7	48
P35d	HC	23.0	0.21	20.5	0.32	19.9	0.28	1.4	0.2	80
P62d	HC	37.3	0.24	21.1	0.33	26.6	0.32	–	52	57

u stands for 10^{-18} m^2.

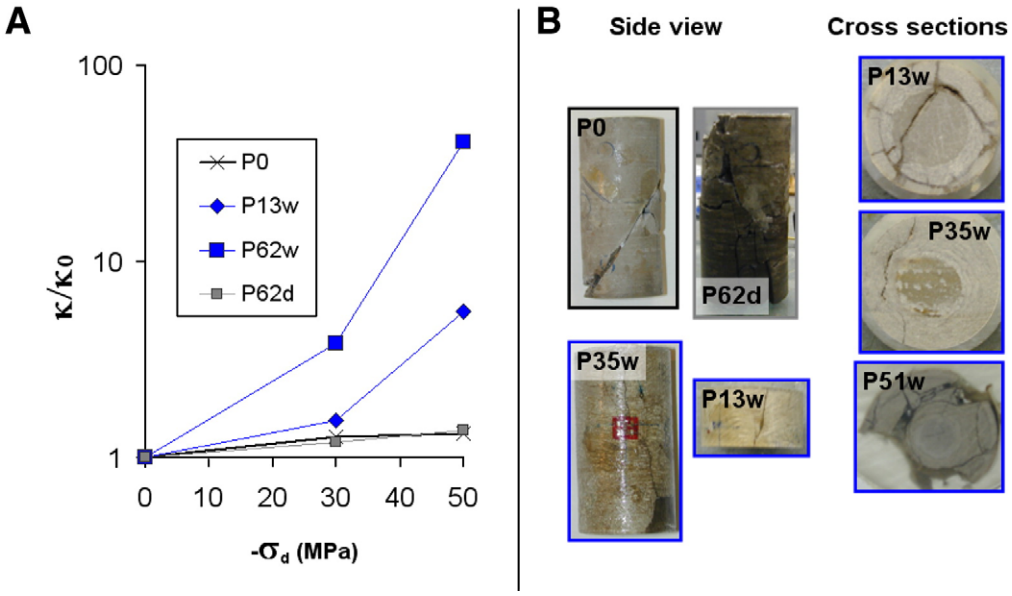

Fig. 8. (A) Water permeability evolution versus deviatoric stress and (B) views on cement samples after fracturing at the end of the tri-axial test.

precipitates and $\xi = 3$ mol/m²/h [19,20] the kinetic constant of the crystal growth. Under these notations, the characteristic time of the crystal growth can be estimated to be $\tau_{crystal} = 1/(V_{vaterite}\ S_p\ \xi)$ which is close to 5 s. On the other hand, the characteristic time of the pore overpressure relaxation, assuming a Poiseuille flow through the capillary, is known to be [26,27] $\tau_{relax} = \zeta(3/4G_m + 1/K_C)$ which is close to 20 s if we consider that the bulk modulus of the carbonate crystal, K_C, is equal to 130 GPa, and that the shear modulus of the cement matrix, G_m, is equal to 15.5 GPa. Thus, τ_{relax} and $\tau_{crystal}$ are found to be on the same order of magnitude. Since this calculation is not based on a real cement microstructure, its aim is not to predict a pore overpressure, but to underline that the kinetic of crystal growth and the kinetic of pore pressure relaxation may be on the same order of magnitude. Thus, that over-pressurisation of in-pore fluid due to carbonation process under downhole condition may happen.

Moreover, cement is a porous medium with a large amount of nano-pores, and, the precipitation is likely to occur within a highly confined medium. Under these conditions, as it is demonstrated in [28], the thermodynamic equilibrium between the crystals that precipitate and the in-pore fluid will be modified. This may result in an increase of the effective pressure transmitted to the cement matrix due to an over-pressurisation of carbonate crystals.

4. Conclusion

The static and dynamic elastic constants, as well as water and gas permeabilities of a set of Portland cement samples carbonated under wet $scCO_2$ at 90 °C and 28 MPa were measured at room temperature. The results clearly show a significant pressure sensitivity of these properties in the samples which develop a carbonation front. This can only be interpreted by the presence of micro-cracks. These micro-cracks, which most likely develop in the vicinity of the front, induce a degradation of the mechanical properties of cement, a decrease in its mechanical strength and an increase of its permeability when deviatoric stress is present. Since under real injection conditions, well-bore cements are expected to carbonate with a progressing carbonation front [10,25], the duration of this transient process appears to be a critical issue both for the cement sealing efficiency and for the long-term well-bore casing integrity. In such a way, elastic wave velocity monitoring of the borehole casings could become an efficient tool to survey the well-bore integrity and predict the evolution of its permeability [29,30].

Acknowledgements

This study was supported by the ANR and EUROGIA in the framework of COSMOS1.

References

[1] V.G. Papadakis, Effect of supplementary cementing materials on concrete resistance against carbonation and chloride ingress, Cement and Concrete Research 30 (2000) 291–299.
[2] B. Johannesson, P. Utgenannt, Microstructural changes caused by carbonation of cement mortar, Cement and Concrete Research 31 (2001) 925–931.
[3] H.-W. Song, S.-J. Kwon, Permeability characteristics of carbonated concrete considering capillary pore structure, Cement and Concrete Research 37 (2007) 909–915.
[4] M. Fernandez Bertos, S. Simons, C. Hills, P. Carey, A review of accelerated carbonation technology in the treatment of cement-based materials and sequestration of CO_2, Journal of Hazardous Materials B112 (2004) 193–205.
[5] J. Jerga, Physico-mechanical properties of carbonated concrete, Construction and Buildings Materials 18 (2004) 645–652.
[6] J. Xiao, J. Li, B. Zhu, Z. Fan, Experimental study on strength and ductility of carbonated concrete elements, Construction and Buildings Materials 16 (2002) 187–192.
[7] G. Rimmelé, V. Barlet-Gouédard, O. Porcherie, B. Goffé, F. Brunet, Heterogeneous porosity distribution in Portland cement exposed to CO_2-rich fluids, Cement and Concrete Research 38 (2008) 1038–1048.
[8] N. Jacquemet, J. Pironon, J. Saint-Marc, Mineralogical changes of a well cement in various H_2S–CO_2(–brine) fluids at high pressure and temperature, Environmental Science & Technology 42 (2008) 282–288.
[9] J. Corvisier, A. Fabbri, F. Brunet, B. Goffé, V. Barlet-Gouédard, A model for CO_2 wells ageing through water/supercritical CO_2/cement interactions, Proceedings of the 3rd International Conference on Coupled T–H–C–M Processes in Geo-Systems, 2008.
[10] V. Barlet-Gouédard, G. Rimmelé, B. Goffé, O. Porcherie, Well technologies for CO_2 geological storage: CO_2-resistant cement, Oil & Gas Science and Technology 62 (2007) 325–334.
[11] R.A. Bruckdorfer, Carbon dioxide corrosion in oilwell cements, SPE 15176 Billings, MT, May 19–21 1986.
[12] D.D. Onan, Effects of supercritical carbon dioxide on well cements, SPE 12593, Permian Basin Oil and gas recovery Conference, Midland, TX, March 8–9 1984.
[13] B.G. Kutchko, B.R. Strazisar, D.A. Dzombak, G.V. Lowry, N. Thaulow, Degradation of well cement by CO_2 under geologic sequestration conditions, Environmental Science & Technology 41 (2007) 4787–4792.
[14] J. Fortin, Y. Guéguen, A. Schubnel, Effects of pore collapse and grain crushing on ultrasonic velocities and V-p/V-s, Journal of Geophysical Research — Solid Earth 112 (2007) B08207-16 p.
[15] D.R. Lide, Handbook of Chemistry and Physics 1999–2000, CRC Press, 1999.
[16] J. Fortin, A. Schubnel, Y. Guéguen, Elastic waves velocities and permeability evolution during compaction of Bleurswiller sandstone, International Journal of Rock Mechanics and Mining Sciences 42 (2005) 873–889.
[17] A. Schubnel, J. Fortin, L. Burlini, Y. Guéguen, Damage and recovery of calcite rocks deformed in the cataclastic regime, in: D. Bruhn, L. Burlini (Eds.), Geological Society of London, Special Publication, vol. 245, 2005, pp. 203–221.

[18] M. Thiery, G. Villain, P. Dangla, G. Platret, Investigation of the carbonation front shape on cementitious materials: effects of the chemical kinetics, Cement and Concrete Research 37 (2007) 1047–1058.
[19] J. Corvisier, F. Brunet, A. Fabbri, S. Bernard, N. Findling, G. Rimmelé, V. Barlet-Gouédard, O. Beyssac, B. Goffé, Raman mapping and numerical simulation of calcium carbonates distribution in experimentally carbonated Portland cement cores, European Journal of Mineralogy (2009).
[20] L. Plummer, E. Busenberg, The solubilities of calcite, aragonite and vaterite in CO_2–H_2O solutions between 0 and 90 C, and an evaluation of the aqueous model for the system $CaCO_3$–CO_2–H_2O, Geochemica et Cosmochemica Acta 46 (1982) 1011–1040.
[21] J.B. Walsh, The effect of cracks on compressibility of rocks, Journal of Geophysical Research 70 (2) (1965) 381–389.
[22] G. Mavko, T. Mukerji, J. Dvorkin, The Rock Physics Handbook, Cambridge University Press, Cambridge USA, 1998.
[23] J.C. Jaeger, N.G.W. Cook, R.W. Zimmerman, Fundamentals of Rock Mechanics, 4th edition, Blackwell publishing, Oxford UK, 2007.
[24] V. Baroghel-Bouny, M. Thiery, F. Barberon, G. Villain, Assessment of transport properties of cementitious materials: a major challenge as regards durability? European Journal of Environmental and Civil Engineering 11/6 (2007) 671–696.
[25] J.W. Carey, M. Wigand, S. Chipera, et al., Analysis and performance of oil well cement with 30 years of CO_2 exposure from the SACROC unit, West Texas, USA, International Journal of Greenhouse Gas Control 75–85 (2007), doi:10.1016/S1750-5836(06)00004-1.
[26] O. Coussy, T. Fen-Chong, Crystallization, pore relaxation and micro-cryosuction in cohesive porous materials, Compte Rendu Mecanique 333 (2005) 507–512.
[27] T. Fen-Chong, A. Fabbri, A. Azouni, Transient freezing–thawing phenomena in water-filled cohesive porous materials, Cold Regions Science and Technology 46 (2006) 12–26.
[28] O. Coussy, Deformation and stress from in-pore drying-induced crystallization of salt, Journal of the Mechanics and Physics and of Solids 54 (2006) 1517–1547.
[29] P. Benson, A. Schubnel, S. Vinciguerra, C. Trovato, P. Meredith, R.P. Young, MOdelling the permeability evolution of micro-cracked rocks from elastic wave velocity inversion at elevated hydrostatic pressure, Journal of Geophysical Research 111 (2006) Art. No. B04202.
[30] P. Benson, P. Meredith, A. Schubnel, Examining the role of void space fabric in the permeability development of crustal rock with pressure, Journal of Geophysical Research 111 (2006) Art. No. B12203.